

How the Shape and Chemistry of Molecular Penetrants Control Responsive Hydrogel Permeability

Matej Kanduč,* Won Kyu Kim, Rafael Roa, and Joachim Dzubiella*

Cite This: *ACS Nano* 2021, 15, 614–624

Read Online

ACCESS |

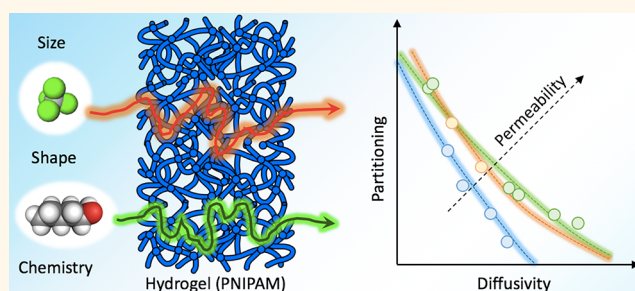
Metrics & More

Article Recommendations

Supporting Information

ABSTRACT: The permeability of hydrogels for the selective transport of molecular penetrants (drugs, toxins, reactants, etc.) is a central property in the design of soft functional materials, for instance in biomedical, pharmaceutical, and nanocatalysis applications. However, the permeation of dense and hydrated polymer membranes is a complex multifaceted molecular-level phenomenon, and our understanding of the underlying physicochemical principles is still very limited. Here, we uncover the molecular principles of permeability and selectivity in hydrogel permeation. We combine the solution–diffusion model for permeability with comprehensive atomistic simulations of molecules of various shapes and polarities in a responsive hydrogel in different hydration states. We find in particular that dense collapsed states are extremely selective, owing to a delicate balance between the partitioning and diffusivity of the penetrants. These properties are sensitively tuned by the penetrant size, shape, and chemistry, leading to vast cancellation effects, which nontrivially contribute to the permeability. The gained insights enable us to formulate semiempirical rules to quantify and extrapolate the permeability categorized by classes of molecules. They can be used as approximate guiding (“rule-of-thumb”) principles to optimize penetrant or membrane physicochemical properties for a desired permeability and membrane functionality.

KEYWORDS: hydrogel, solvation, diffusion, permeability, selectivity, molecular dynamics simulation



In the past decade, we witnessed considerable research progress in hydrogels and their applications, owing to the advances in materials science, nanotechnology, polymer physics, and fabrication techniques.^{1–3} Hydrogels are cross-linked polymer networks containing a considerable amount of water. How much water a hydrogel contains depends on its chemistry, the density of cross-linkers, and environmental parameters, such as temperature. The attention has in recent years shifted toward stimuli-responsive hydrogels, popularly known as “smart” or “active” materials, which undergo a rapid and reversible structural transformation in response to an environmental stimulus (e.g., temperature or pressure).^{2,4,5} They have become building blocks in a broad repertoire of biomedical, pharmaceutical, and other applications, including chemical separation,⁶ biosensors,⁷ nanofiltration,^{8,9} active interfaces,¹⁰ biomedical devices,^{11,12} nanocatalysis,^{13–16} and—maybe the most eminent example—controlled drug delivery.^{3,17,18} In the latter, hydrogels can be designed to selectively encapsulate and release particular types of pharmaceuticals in a controllable way. Related aspects are used in “programmable” nanoreactors, where catalytic nano-

particles are confined in a permeable hydrogel that shelters and controls the catalytic process.^{13,14,19–22} Most of these applications exploit a tunable permeation of small target molecules (referred to as penetrants) through a responsive hydrogel. Permeation is driven by a chemical potential gradient of penetrants, caused for instance by a concentration difference Δc on both sides of the hydrogel. In this case, the permeation flux density is given as $j = P(\Delta c/L)$, where L is the thickness of the hydrogel and P stands for permeability, which will be the central quantity of discussion in this work. Permeability defined in this way is an intensive quantity with units of a diffusion coefficient; however, the definitions vary among different fields. Based on the well-established solution–

Received: July 28, 2020

Accepted: December 28, 2020

Published: December 31, 2020



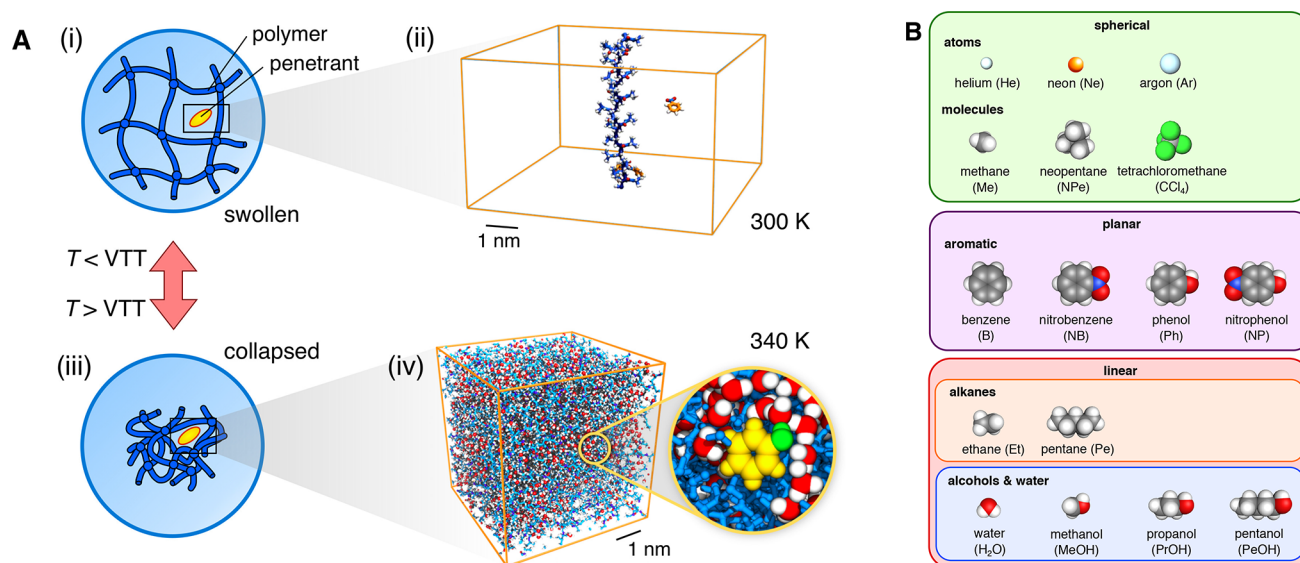


Figure 1. (A) Atomistic modeling of PNIPAM hydrogels with penetrants. Top: (i) a swollen network, where adjacent chains are far apart (relevant for temperatures below the VTT), is simulated as (ii) an infinitely long chain to study adsorption³⁸ (water not shown for clarity). Bottom: (iii) a collapsed hydrogel (relevant for temperatures above the VTT) is modeled as (iv) a dense aggregate of PNIPAM polymers containing penetrants (an example of phenol is shown in yellow).^{39,40} (B) Penetrant molecules in our study classified into three groups based on shape.

diffusion theory,^{23,23–25} the permeability can be written as the product of the diffusion coefficient (diffusivity) D of the penetrant and its partition ratio (partitioning) in the material K , as

$$P = KD \quad (1)$$

The partition ratio is the concentration of the penetrant in the hydrogel relative to that in bulk water in thermodynamic equilibrium, and it therefore tells how much of a given solute ends up in each phase. The theoretical understanding of diffusion and partitioning individually is much more established than of permeability, which is why most theoretical and modeling efforts tackle the permeability through the diffusion and partitioning of a given system.^{26–28} Furthermore, determining P directly in simulations by measuring fluxes is often unachievable. As a matter of fact, D and K are quite universally (anti)correlated for a wide spectrum of penetrants in a given material.^{26,27,29} This means that those penetrants that are well absorbed by a given material diffuse more slowly therein than those that are absorbed less. Consequently, diffusivity and partitioning are in competition, and their opposing effects are subject to cancellations in the resulting permeability (eq 1). Consequently, the permeability significantly depends on details of D and K , as has been shown by mesoscale models.^{28,30} This clearly hints that a precise, even molecular-level understanding of D and K is crucial to understand the permeability.

There were several attempts to devise heuristic rules for permeability based on experimental observations and subsidized by phenomenological theories.^{31,32} The research on penetrant transport has a venerable history, resulting in a plethora of theories based on different premises.^{33,34} Although many of them have been successful in rationalizing the diffusivities of several penetrants, most have shortcomings, as they either are not really atomistic or assume a certain molecular behavior in an *ad hoc* manner.³⁵ The problem is that permeation is a complex multiscale phenomenon; thus picking the right theory is a formidable challenge.³⁶ For instance, the

role played by the shape and the “chemistry” (*i.e.*, hydrogen bonds, polarity, charges) of penetrating molecules is still not understood. A suitable method that can assist in a theoretical understanding is molecular simulations, but which are nowadays unfortunately still limited in this field because of the computationally intensive nature needed for studying permeability.

In this work, we elucidate the role of the penetrant’s shape and polarity in the permeability as resolved from comprehensive molecular dynamics (MD) simulations of a poly(*N*-isopropylacrylamide) (PNIPAM) hydrogel. PNIPAM is the most prominent and most studied thermoresponsive polymer, owing to its biocompatibility and the volume transition temperature (VTT) close to human body temperature, and it serves as the prototypical model system for many studies today.³⁷ We combine the simulation data from this work with the data from our recent studies.^{38–41} We separately analyze the partitioning and diffusivity of different penetrants in swollen and collapsed states of PNIPAM, which enables us to evaluate the permeability based on the solution–diffusion model. To understand the background of the permeability in the collapsed state, we rationalize each of the two components of the permeability—the diffusivity and the partitioning—by semiempirical scaling relations.

RESULTS AND DISCUSSION

Modeling Approach. PNIPAM-based hydrogels undergo a volume transition (*i.e.*, a transition between the swollen and collapsed state) at the VTT of around 305 K (32 °C).³⁷ In order to treat the two states with computer simulations, we use two distinct models established before, which are suitable for hydrogels with low cross-linker concentrations,^{38,39} as shown in Figure 1A. The model for the swollen state is a single stretched and periodically replicated polymer chain in a box of water at 300 K (below the VTT); see Figure 1A(i, ii). This chain can be considered as a segment of a swollen polymer network, where neighboring chains are far apart and do not

interfere with each other, feasible for low cross-linker concentrations. The model for the collapsed state (Figure 1A(iii, iv)) consists of aggregated polymeric chains (20 monomer units long) at 340 K (above the VTT).³⁹ Because the model does not have cross-linkers, it is suitable for a collapsed hydrogel with very low (few percents) cross-linker concentrations, in which the cross-linkers do not pose major geometrical constraints during the collapse. We examine the permeability of various penetrant molecules in PNIPAM hydrogels, with the focus on the collapsed state. We first briefly tackle the swollen state—for which the results can be easily interpreted—and then, for the rest of the article, concentrate on the collapsed state, which yields much more complex permeability behavior.

We explore the behavior of different kinds of penetrants, which we categorize into three groups based on their shape and chemistry, as shown in Figure 1B. The first group consists of spherical penetrants, featured by equal lengths of their principal axes. The second group includes planar (aromatic) molecules, with one principal axis shorter than the other two. Here, nitrobenzene and nitrophenol are particularly popular in model reactions in nanocatalysis,^{42,43} used also in connection with PNIPAM hydrogels.¹⁴ Finally, the third group constitutes linear (rod-like) molecules, such as alkanes and alcohols, with one axis longer than the other two. For simplicity, we also place the water molecule into the latter group.

The simulation data for the analysis are partially taken from our previous studies^{38–40} and partially supplemented by simulations in this work (see the Methods section for details).

Swollen State. The single-chain model of a swollen state (Figure 1A(ii)) enabled us to study the adsorption of molecules onto the polymer.³⁸ In the linear regime of adsorption, valid for concentrations of molecules up to around $c_0 \approx 10$ mM,³⁸ the number of adsorbed molecules per monomer is $N_{\text{ads}} = \Gamma_m^* c_0$, where Γ_m^* is referred to as an adsorption coefficient. We can then predict the partitioning in a hypothetical swollen gel (denoted by the subscript “s”) as^{38,41}

$$K_s = 1 + n_m \Gamma_m^* \quad (2)$$

where n_m is the number density of monomers in the hydrogel. The number density can be easily linked to the polymer volume fraction $\phi = (\pi R_0^2 l_m) n_m$, where the factor in the parentheses is the volume of one monomer, with $R_0 \approx 0.5$ nm being the effective radius of the PNIPAM chain and $l_m = 0.265$ nm the longitudinal size of the monomer.³⁸ Equation 2 can be further extended to include the adsorption on hydrogel cross-linkers, which could have either an enhancing or diminishing effect, as investigated elsewhere.⁴⁴ In order to keep the model simple, we will neglect explicit cross-linker contributions in the following (*i.e.*, considering hydrogels with a low cross-linker density).

This single-chain model does not lend itself to study diffusion in a swollen network. Diffusion studies in swollen networks within the all-atom framework are very scarce, one of the reasons being that they are computationally expensive because of a huge amount of simulated water and, more importantly, that they are not expected to be particularly illuminating compared to other, more generic and cheaper coarse-grained models. We will therefore resort to theoretical predictions for rough estimations of the diffusion coefficients. Fortunately, diffusion theories are typically successful for swollen networks of low polymer volume fractions.^{33,34,36}

We first recall that the diffusion in water is described by the Stokes–Einstein equation,⁴⁵

$$D_w = \frac{k_B T}{6\pi\eta a_w} \quad (3)$$

based on the molecule’s Stokes radius (a_w) and the water viscosity (η), where k_B is the Boltzmann constant and T the temperature. A swollen polymer network can pose steric, hydrodynamic, and other nonsteric interactions on the diffusing penetrants.^{46,47} A simple and popular model that treats the steric hindrance effect is the Mackie–Meares model,⁴⁸ which we will use in our approach:

$$D_{\text{st}} = D_w \left(\frac{1 - \tilde{\phi}}{1 + \tilde{\phi}} \right)^2 \quad (4)$$

Here, the diffusion coefficient in bulk water, D_w , is attenuated by a steric factor, in which the effective polymer volume fraction is defined as $\tilde{\phi} = \phi(1 + a_w/R_0)^2$ and corresponds to the excluded volume of the chain including the effective penetrant’s radius, a_w .

Nonsteric effects are more challenging to incorporate into the theory. In a simplified picture, a steric network decorated by an attractive potential engenders an adsorption and trapping of the penetrant, which in turn prevents its diffusion while it is adsorbed.⁴⁹ This notion leads to a simple relation, proposed and verified by coarse-grained simulations,³⁰

$$D_s = D_{\text{st}} f_{\text{free}} \quad (5)$$

where D_{st} is the diffusion coefficient in the steric network (*i.e.*, without the attractive part, as given for instance by eq 4) and f_{free} is the fraction of time the particle is not adsorbed and can freely diffuse between the chains in the network. This fraction can be computed as the ratio of the number of “free” particles and the total number of particles in the gel, $f_{\text{free}} = N_{\text{free}}/N_{\text{in}}$. The latter follows from the definition of partitioning as $N_{\text{in}} = K_s c_0 V$, whereas the number of free penetrants in the gel can be estimated from the volume that is not occupied by the polymer (with the effective excluded radius $R_0 + a_w$); thus $N_{\text{free}} = c_0 V(1 - \tilde{\phi})$. With this, the fraction of free particles can be expressed as $f_{\text{free}} = (1 - \tilde{\phi})/K_s$, such that eq 5 then becomes

$$D_s = \frac{D_w (1 - \tilde{\phi})^3}{K_s (1 + \tilde{\phi})^2} \quad (6)$$

The corresponding permeability in the swollen state, $P_s = K_s D_s$, is then

$$P_s = D_w \frac{(1 - \tilde{\phi})^3}{(1 + \tilde{\phi})^2} \quad (7)$$

As simple as this model may be, it suggests that the permeability depends foremost on the polymer volume fraction and to some extent on the penetrant’s size *via* the excluded-volume principle. The “chemistry” of the penetrant, that is, its specific interaction with the polymer, has entered the partitioning and diffusivity in reciprocal ways and canceled out and is thus irrelevant for the permeability.

Collapsed State. We now move on to the core of this work, namely, to the collapsed state (Figure 1A(iv)). The amount of sorbed water between the aggregated chains is chosen such that it matches the chemical equilibrium of bulk water, which for the used model is around 20 wt % (somehow

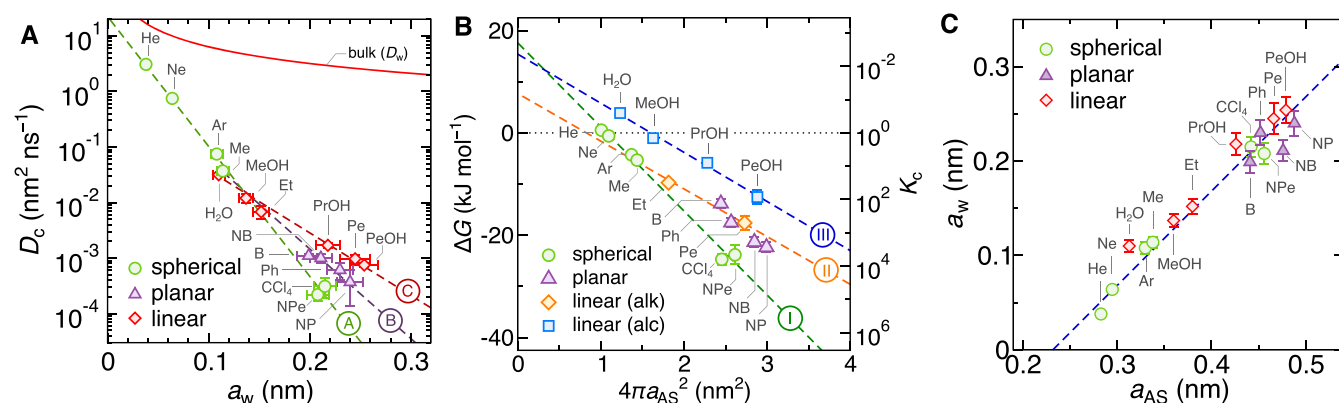


Figure 2. (A) Diffusion coefficients of penetrants in the collapsed PNIPAM polymer (at 340 K) versus their Stokes radii in bulk water, categorized into three groups based on their shape (see Figure 1B). The dashed lines are fits of eq 8 to the three different categories, denoted as A, B, and C (see Table 1). The red solid line is the diffusion coefficient in bulk water (D_w), given by eq 3. (B) Transfer free energies of penetrants from water into the collapsed PNIPAM (left scale) and the corresponding partition ratio (right scale) versus the accessible surface area (ASA), categorized into four groups of penetrants based on the shape and polarity. The dashed lines are fits of eq 10 to three different categories, denoted as I, II, and III; planar penetrants excluded (see Table 1). (C) Correlation diagram of a_w versus a_{AS} for the simulated penetrants. The blue dashed line is the fit of eq 11 to the data points.

below experimental estimates, of around 30 wt %^{17,50–53}). This makes the polymer volume fraction around $\phi \approx 0.8$. Water is very nonuniformly distributed throughout the phase in a form of irregular nanoscopic clusters, as is common to dense amorphous polymer structures in general.^{26,54,55}

Diffusion in this packed polymer structure advances *via* the hopping mechanism, identified in simulations^{35,56–58} as well as experiments,^{59,60} where a penetrant performs jumps from one local cavity formed by the chains to another local cavity through short-lived water channels created by thermal fluctuations.³⁹ This makes the diffusion a barrier-crossing phenomenon.³⁹ In Figure 2A we plot the diffusion coefficient in the collapsed state D_c (“c” standing for collapsed) against the penetrant’s size, characterized by the Stokes radius a_w (defined through eq 3 from a measured D_w of the penetrant in water). In our previous study, we already noted that diffusion coefficients in this system very roughly follow an exponential dependence,³⁹ but now, with the extended assortment of penetrants, it is clear that the data points of larger penetrants (beyond methane) start to scatter from a single decreasing trend.

Notably, by classifying the penetrants (see Figure 1B) as spherical (green circles), planar (purple triangles), and linear (red diamonds), the diffusivity of each group individually follows very well an exponential dependence:

$$D_c = D_0 e^{-a_w/\lambda} \quad (8)$$

with the prefactor D_0 and the decay length λ as free parameters. When moving through the groups of planar or linear penetrants toward larger sizes a_w , the penetrants are effectively becoming larger only in one dimension, whereas the other two dimensions remain nearly constant. For this reason, we also include the methane data point (Me) as the starting point (having one carbon atom) into the fitting procedures. The fitting parameters D_0 and λ are listed in Table 1.

With an increasing size, the course of diffusion coefficients first follows the exponential dependence of the spherical geometry and then forks into three branches at around the size of the methane molecule, whence also nonspherical structures are realizable. Thereby, planar and even more so linear penetrants diffuse significantly faster than spherical penetrants

Table 1. Fitting Parameters in Eqs 8 and 10, Given in the Following Units: D_0 ($\text{nm}^2 \text{ns}^{-1}$), λ (nm), ΔG_0 (kJ mol^{-1}), and γ_0 ($\text{kJ mol}^{-1} \text{nm}^{-2}$)

diffusion fits (Figure 2A)			
#	group	D_0	λ
A	spherical	22.4	0.0186
B	planar + Me	2.34	0.0270
C	linear + Me	0.504	0.0386
free energy fits (Figure 2B)			
#	group	ΔG_0	γ_0
I	spherical	17.6	−16.4
II	linear (alkanes) + Me	7.71	−9.33
III	linear (alcohols) + H ₂ O	15.4	−9.60

of equal Stokes radii. The influence of shape on diffusion in dense polymers is poorly understood.³⁶ In our case, we believe the reason lies in the hopping through transient channels, where the smallest cross section of the penetrant is the determining dimension. Namely, molecules preferably move through narrow channels in the direction of the smallest cross section. Clearly, spherical particles have the largest cross section among all three geometries for a given Stokes radius, therefore the smallest diffusion coefficient D_c in the hydrogel. On the other hand, the Stokes radius is approximately equal to the mean of all three principal axes of the penetrant;^{45,61} thus all cross sections contribute similarly to diffusion in water.

The polymer–penetrant interaction (the chemical type) seems not to be a prevailing factor in diffusion. The reason could be that during a hopping event the coordination of the solvation shell of a penetrant is not significantly perturbed,³⁹ and consequently the free energy changes are much smaller than steric interactions of local trapping. An emerging important conclusion from Figure 2A is that for a given shape category the diffusion coefficients in our system decay exponentially with the penetrant’s size.

Even though some studies suggest such a diffusivity scaling in dense systems,^{62–64} most of them propose or assume exponential decays with a square or cube of the penetrant size.^{33,34} In the Supporting Information (SI) we show that these other two alternatives give significantly worse fits to our

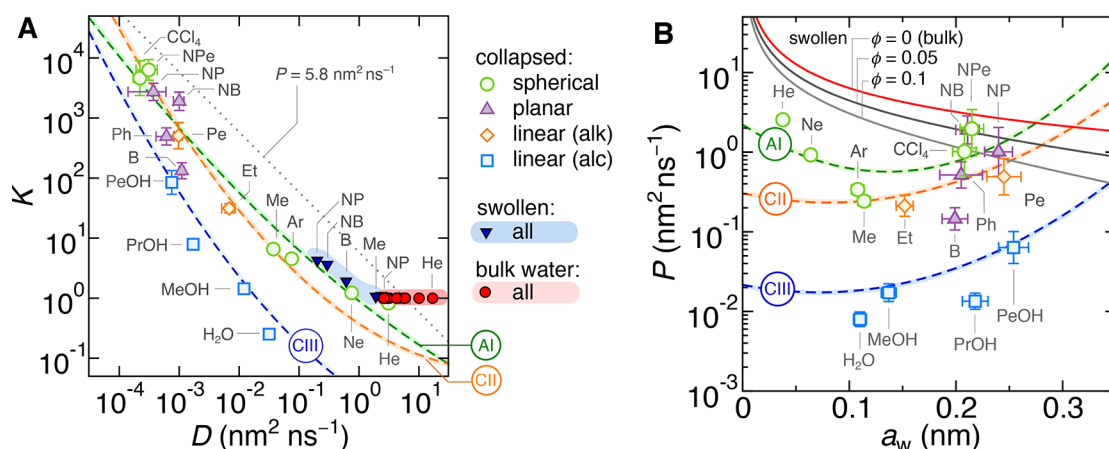


Figure 3. (A) Partitioning–diffusivity correlation diagram. The data points in the red-shaded region correspond to bulk water ($T = 300$ K), the points in the light-blue-shaded region correspond to the swollen state ($\phi = 0.1$, $T = 300$ K; shown only for Me, B, NB, NP), and the remaining data points correspond to the collapsed state ($\phi \approx 0.8$, $T = 340$ K). The gray dotted line is the iso-permeability line with the constant permeability of $P = 5.8 \text{ nm}^2 \text{ ns}^{-1}$. The dashed lines are predictions of the semiempirical relation eq 12 using parameter sets from Table 1. (B) Permeability as a function of the penetrant size a_w . The data points are MD simulations for the collapsed state. Solid lines are theoretical results (eq 7) of the permeability in bulk water (red, $\phi = 0$) and swollen states for different ϕ (gray), while the dashed lines are predictions of the semiempirical relation eq 13 for the collapsed state using the same parameter sets as in panel A.

data than eq 8. Particularly the square scaling, $\ln D_c \propto -a_w^2$, is deeply rooted in the polymer community. For instance, it follows from the free-volume theory^{33,65,66} and serves as the basis for the well-established framework for gas separation by polymer membranes by Freeman.⁶⁷

The question on diffusivity-size scaling is complex and still under debate, as it seems that it depends not only on the polymer but also on the temperature regime. Kumar, Zhang, and co-workers used coarse-grained, implicit-solvent models and identified three generic regimes of diffusion in polymers.^{68–70} While the diffusivity of very small penetrants indeed follows $\ln D_c \propto -a_w$, it is not activated. For larger penetrants at temperatures above the glass transition temperature (T_g), diffusivity follows a power-law dependence with size, and below or near T_g , the diffusion is activated (*i.e.*, the diffusivity scales with temperature as $\ln D_c \propto -E_a/k_B T$, where E_a is the activation energy). Coarse-grained models seem to predict $E_a \propto a_w^2$, which contrasts our linear scaling in the all-atom model.⁷⁰ Our system lies slightly above the glass–rubber crossover, with $T/T_g \approx 1.2$ (see SI), the segmental relaxation is on the order of the penetrant caging time (see SI), and the diffusion is activated.³⁹ This classifies the system into the activated diffusion regime according to Kumar, but with a different size scaling. Importantly, our polymer contains water, and penetrants transit through “wet” water channels, rather than through “dry” channels as is the case in coarse-grained approaches. Whether the difference is due to water is hard to ascertain, but Zhang and Schweizer showed that a coupled dynamics in dense liquids indeed results in an exponential size dependence.⁶⁴ Remapping their hard-sphere model to ours (see the SI), yields, in fact, quantitatively very similar values for the decay length λ given in eq 8.

The other important question is how do penetrants solvate in the hydrogel and what is their partition ratio. Using simulations, we compute the transfer free energy ΔG of penetrants from water into the gel (see Methods), which is related to the partition ratio K_c (in infinite-dilution limit of penetrants) as

$$K_c = e^{-\beta \Delta G} \quad (9)$$

where $\beta = 1/k_B T$. In Figure 2B we show the transfer free energies *versus* the accessible surface area (ASA) of the penetrants, $4\pi a_{AS}^2$, a common measure in analyzing solvation. Here, a_{AS} is the equivalent spherical radius of the ASA. See the Methods section for the definition of ASA. The right scale in Figure 2B shows the calculated K_c from eq 9.

For solvation, not only the size and shape but also the chemical character of a penetrant matters. We therefore divide the linear penetrants further into nonpolar (alkanes) and polar molecules (alcohols and water), the latter featuring the hydroxyl (OH) group (see Figure 1B). As noted before, an OH group in aromatic penetrants does not make much of a difference in the solvation.⁴⁰ This is presumably because an OH group bound to a phenyl ring (to an unsaturated sp^2 carbon) is less polar than in alcohols (bound to a saturated sp^3 carbon),⁷¹ which is reflected also in different partial charges in the used force field.⁷²

The results for the transfer free energy can be nicely described by the ASA and an effective molecular surface tension γ_0 ,^{40,73,74}

$$\Delta G = \Delta G_0 + 4\pi\gamma_0 a_{AS}^2 \quad (10)$$

as shown by solid dashed lines in Figure 2B (fitting parameters are listed in Table 1). For the fitting of linear alkanes, we include the methane data point as the limiting penetrant size with one carbon atom. The coefficient γ_0 in eq 10 can be in a way interpreted as the difference in the penetrant–PNIPAM and penetrant–water surface tensions, whereas the sign depends on the transfer direction.⁴⁰ Alcohols (including water) feature the same γ_0 (within numerical accuracy) as linear alkanes because the alkyl tails are identical in both. However, the OH group in alcohols, which has a higher affinity to water than to PNIPAM, makes the free energies of alcohols by around 8 kJ/mol higher than those of the alkanes (see Table 1). This, for instance, explains why hydrophobic dyes partition more in PNIPAM-like networks than hydrophilic ones.⁷⁵ Aromatic molecules in this respect behave similarly to the linear alkanes, and thus we refrain from fitting their data. Interestingly, spherical molecules seem to solvate better in

PNIPAM than linear or planar molecules of similar ASA. The cause could lie in curvature effects—linear and planar molecules have one of the principal curvatures significantly larger than the other—as was shown for solvation of hydrophobes in water.⁷⁶ Most importantly, the penetrant size is the dominant factor that determines the affinity to the hydrogel; that is, larger penetrants are more condensable and more soluble than smaller penetrants, known also from pervaporation in membranes.⁷⁷

Solvation of small solutes is—similar to diffusivity—a debated topic, and alternatively to area scaling in eq 10, one can assume volume scaling or even a superposition of both.⁷⁸ The volume scaling has rationale in the entropic solvation of small spherical cavities, being inversely proportional to the compressibility of the medium.⁷⁹ This suggests better solvation in a less compressible medium, which is in our case the water phase (see the SI); thus it cannot explain our trends. The molecular heterogeneity of the PNIPAM phase, featuring polymer interfaces and hydrated voids, further convolutes the solvation. Our choice of the scaling with ASA (eq 10) is empirical and performs better than the scaling with volume, as we show in the SI. Nevertheless, both choices lead to qualitatively the same conclusions concerning permeability later on, since both scale with a higher power of the penetrant size than the diffusivity.

We used different definitions of penetrants' sizes for the analyses of diffusivity (a_w) and solvation (a_{AS}), which are in accordance with respective standard practices. Fortunately, the correlation plot of both in Figure 2C reveals a clear, almost one-to-one mapping in the form of

$$a_w = a_{AS} - \Delta a \quad (11)$$

with $\Delta a = 0.233$ nm, shown by the dashed line. However, neither of the two definitions accurately reflects the actual, physical size of an atom or a molecule. The size is traditionally best expressed, at least for atoms, by the van der Waals radius. The latter is namely $a_{AS} - 0.14$ nm, thus approximately right between a_w and a_{AS} .

Permeability. We now investigate to what extent are partitioning and diffusivity related and what role do they play in the permeability. For a start, we compose a partitioning–diffusivity correlation diagram, shown in Figure 3A. The diagonal gray dotted iso-permeability line $KD = 5.8$ nm² ns⁻¹ (the water diffusivity in bulk water) serves for orientation. All molecules in bulk water, shown by red circles in a red-shaded domain, lie on a horizontal line in the diagram (with $K = 1$).

For the swollen state we choose the polymer volume fraction $\phi = 0.1$, which is typical for PNIPAM hydrogels with 5 mol % of cross-linkers.^{14,44} We obtain the partition coefficient K_s from eq 2 using Γ_m^* from single-chain simulations³⁸ and estimate the diffusion coefficient D_s from the theoretical prediction eq 6. The results for a few selected penetrants are plotted in the bottom-right corner of the diagram, encompassed in a blue-shaded domain. As seen, the swollen state covers quite a tiny region of the entire diagram, and the data points lie roughly on the same iso-permeability line. Clearly, the calculations for the swollen state are based on simple theoretical assumptions, and their sole aim is to demonstrate a mild variance in the diagram in contrast with the collapsed state, which we extensively discuss in the following.

In the collapsed state, the penetrants are much more broadly distributed across the diagram, with both K_c and D_c spanning over around 4 orders of magnitude. We can clearly notice an

anticorrelation between K_c and D_c for all categories of penetrants, which leads to cancellation effects in the resulting permeability.

To elucidate this important observation, we return to the established semiempirical rules for D_c (eq 8) and K_c (eq 10): we merge both relations by eliminating the penetrant sizes a_w and a_{AS} , respectively, by using eq 11. This brings us to the following relation between K_c and D_c :

$$\ln K_c = -\beta\Delta G_0 - 4\pi\beta\gamma_0\lambda^2 \left(\ln \frac{D_c}{\tilde{D}_0} \right)^2 \quad (12)$$

where we have abbreviated $\tilde{D}_0 = D_0 \exp(\Delta a/\lambda)$. This equation directly demonstrates the partitioning–diffusivity anticorrelation; note that in the relevant regime $\ln(D_c/\tilde{D}_0) < 0$. This prediction is plotted in Figure 3A as three dashed lines using different combinations of our parameter sets. First, for spherical penetrants we use the diffusivity set A and the free energy set I from Table 1 (green line, denoted as AI). The orange line (CII) combines the parameters from sets C and II and describes the trend of linear alkanes. Finally, the blue line (CIII) describes the trend of alcohols and water. All three trends are thus nicely captured by the semiempirical relation.

In Figure 3B we plot the permeabilities against the penetrants Stokes radius, a_w . Theoretical predictions for swollen states (eq 7) are shown by gray solid lines (for $\phi = 0.05$ and 0.1), as well as for bulk water ($\phi = 0$, red line). Permeabilities of the simulated penetrants (categorized into the same four groups as in panel A) in the collapsed state, P_c , follow from the product of K_c and D_c as dictated by the solution–diffusion theory, eq 1.

To illuminate the nature of the above outcomes, we again use the semiempirical relations eqs 8 and 10, to arrive at the expression for the permeability:

$$P_c = D_0 \exp \left[-\beta\Delta G_0 - 4\pi\beta\gamma_0(a_w + \Delta a)^2 - \frac{a_w}{\lambda} \right] \quad (13)$$

The predictions are shown by dashed lines in Figure 3B for the same three parameter sets as in panel A. The lines indeed catch the trends of the data points.

The semiempirical concepts that follow from eq 13 indicate the following: diffusion coefficients for a given shape and chemical character of molecules decay exponentially with the size, whereas partitioning rises exponentially with the square of the size. This makes the permeability nonmonotonic in terms of the penetrant's size, with the minimum at

$$a_w^{(\min)} = -\frac{k_B T}{8\pi\gamma_0\lambda} - \Delta a \quad (14)$$

For spherical molecules the calculated minimum is at $a_w^{(\min)} \approx 0.14$ nm (slightly larger than the methane molecule), which can indeed be observed from the MD data. For linear molecules, on the other hand, the hypothetical minimum $a_w^{(\min)} \approx 0.1$ nm is smaller than the smallest linear molecule (water) in our study; therefore, the permeability only monotonically increases with size.

Thus, the diffusivity is more important for smaller penetrants, and, therefore, quite universally, the permeability for small molecules is rather low (except for the smallest ones, He and Ne). For larger penetrants ($a_w > a_w^{(\min)}$), the partitioning is gradually becoming more decisive for the permeability. In fact, our penetrants, with the size range

between 0.05 and 0.25 nm, lie around the minimum (eq 14), where the permeability is only mildly dependent on the size. Contrarily, in the materials in which $\ln D_c \propto -a_w^2$, the size effect in D_c and K_c cancels out completely in P_c , and therefore makes the filtration on the basis of size not possible. Instead, the permeability is much more affected by the chemistry; note an order of magnitude or two lower permeabilities for polar penetrants (alcohols) compared with the other molecules of similar sizes. Thus, the collapsed state can selectively filter molecules based on their chemistry much more efficiently than on their size. Filtering on the basis of chemistry seems always operative in dense polymer systems, as we cannot foresee a mechanism that would completely compensate D_c and K_c on the penetrant's chemistry basis. This demonstrates the importance of the chemistry-specific penetrant–hydrogel interactions, which are lacking in simple theories and generic coarse-grained models.

Finally, we note that the substantial cancellations of the diffusivity and partitioning in PNIPAM is in considerable contrast to Overton's rule in lipid bilayers (often egg lecithin). There, the strong dependence of P on a solute type is interpreted as the dependence of K on the solute type because diffusivity there is often only weakly dependent upon solute.^{80,81}

Polymer Volume Fraction and Temperature. For the end, we take a look at how the permeability through the hydrogel changes with the polymer volume fraction and temperature. In Figure 4 we show the permeability for three

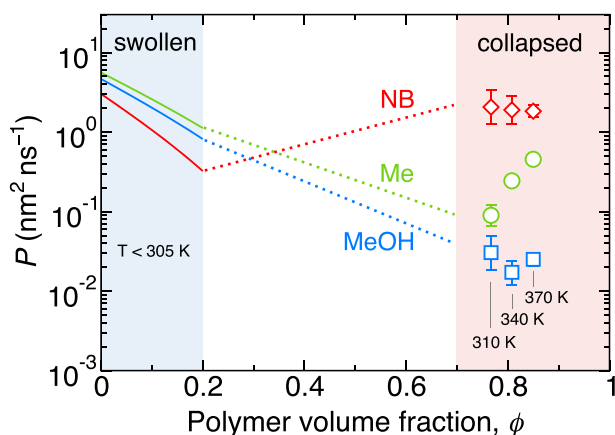


Figure 4. Permeability as a function of polymer volume fraction for three penetrants: methane (Me), methanol (MeOH), and nitrobenzene (NB). The solid lines are the theoretical predictions from eq 7, relevant for swollen states ($\phi < 0.2$, blue region). The symbols are simulation results of the collapsed model (red region), performed at three different temperatures and the corresponding polymer volume fractions and calculated as $P_c = K_c D_c$. The dotted lines serve as guides to the eye for connecting the swollen and collapsed states.

selected penetrants: methane, methanol, and nitrobenzene. The blue- and the red-shaded areas indicate roughly the volume fractions relevant for swollen and collapsed hydrogel states, respectively, whereas the white area is a transition region, not stable in reality. The theoretical curves for swollen states (eq 7) lie close to each other; they depend only on the penetrant size. For the collapsed state, we added data for 310 and 370 K. Note that each temperature corresponds to a different polymer volume fraction, such that the sorbed water

is in equilibrium with bulk. The permeability now becomes significantly penetrant-specific, and even the order changes: nitrobenzene, with the lowest permeability among the three molecules in the swollen state, becomes the most permeable one in the collapsed state.

The volume-fraction dependence (and likewise the temperature dependence) of P_c in the collapsed state is very nontrivial. On the one hand, our previous study showed that D_c universally increases with temperature for all penetrants by the same factor;³⁹ note that the temperature dependence is non-Arrhenius as the temperature changes also the hydration and the polymer volume fraction. But on the other hand, temperature dependence of the partitioning K_c is much more penetrant-specific. For small nonpolar molecules, K_c is almost independent of temperature. For this reason, P_c for methane increases with temperature at the expense of an increasing $D_c(T)$. But polar penetrants and nitrobenzene solvate worse in PNIPAM at higher temperatures (in a more hydrophobic environment), and the decreasing $K_c(T)$ compensates the increasing $D_c(T)$.

It can be clearly seen that the collapsed state becomes extremely selective. For instance, a swollen hydrogel is comparably permeable to nitrobenzene and methanol, whereas as it collapses, it stays similarly permeable to nitrobenzene, but it practically completely blocks methanol (the permeability plummets by 2 orders of magnitude). One might naively expect the opposite, as nitrobenzene is larger than methanol and it diffuses more slowly in the collapsed state, yet the decisive factor for this switch is rather the partitioning, controlled by the polar character. Tunable permeabilities in responsive PNIPAM-based hydrogels have been experimentally demonstrated in different contexts (e.g., in controllable glucose uptake⁸² or switchable catalytic reactions of nitrobenzene and ionized nitrophenol¹⁴).

So far, we have learned that in the collapsed state the chemical character, shape, and size of the penetrant come much more to the fore than in swollen states. The collapsed state exhibits much richer interplay between the molecular interactions, making it much more selective for permeation (or filtration) of molecules. In other words, controlling the water content is key in determining the permeation and selective properties of a hydrogel, possibly by varying the extent of charge functionality, cross-linking, or polymer architecture and morphology. This is also the reason that highly selective commercially available membranes sorb relatively little water.⁸³

In the end, Figure 4 also shows that permeability can change nonmonotonically with the polymer volume fraction, exhibiting minima and maxima (for the case of nitrobenzene). The notion of permeability maximization has been recently observed in generic coarse-grained models,²⁸ but in this study, it is demonstrated in an atomistic model with a real hydrogel chemistry. The knowledge about how to sufficiently tailor and optimize the permeability is paramount to a rational design of applications in materials science. For instance, the ability to selectively transport solvent and solute molecules for the desired material function has been a grand challenge in materials science over the past decade.^{84,85}

CONCLUSION

Our results, based on the solution–diffusion model and comprehensive molecular dynamics simulations, offer a well-grounded molecular basis for permeability in hydrogels. We witnessed strong anticorrelations between the diffusivity and

partitioning in all states of the hydrogel and, consequently, large cancellations in the resulting permeability. In swollen states, the permeability only weakly depends on the penetrant type, meaning that there is little practical control over the permeability and selectivity. On the contrary, the permeability in the collapsed and dehydrated polymer state is extremely sensitive to tiny features of the penetrant, such as its shape, size, and chemical character, making collapsed states highly selective to tiny differences between molecules.

Strikingly, the outcomes clearly defy many well-accepted transport theories in this field, which is a reason for revisions and improvements of the current theoretical foundations in dense polymer architectures. With the gained molecular-level insights we formulated semiempirical rules for permeability of molecular penetrants of various physicochemical types for a certain membrane material. These rules are also useful to predict and understand how and why already tiny chemical modifications, such as methylation or hydroxylation, change the permeability and selectivity, in some cases even by an order of magnitude. We believe that our results will help to revise and improve the current theoretical foundations, which is crucial for a rational design of soft materials for molecule-selective transport and function. We should also mention that charged penetrants, not covered in this study, impose an additional layer of complexity, stemming from interfacial effects of water clusters.⁸⁶

Finally, insights from theoretical modeling are not only limited to synthetic hydrogels but could probably also help to understand various hydrogels found in nature. Many biological gels (e.g., mucus, the extracellular matrix, biopolymers in nuclear pores, bacterial biofilms, vitreous humor) enable a selective exchange of molecules, allowing a passage of particular molecules while rejecting others.⁴⁶ The underlying principles of how they manage to do this are still unknown.

METHODS

We complement the simulation data for diffusivity and solubility/partitioning in the collapsed state (Figure 1A(iv)) from the previous studies^{39,40} by the following data. Diffusion coefficients (D_c): CCl_4 , NPe, Pe, Ph, PrOH, PeOH. Transfer free energies (ΔG): Ar, CCl_4 , NPe, Pe, PeOH. We use the same methods as in detailed described in refs 39 and 40, which we, for the reader's convenience, briefly recap in the following. On the other hand, no additional simulations were performed for the swollen state (Figure 1A(ii)) in this study.

Atomistic Model. The collapsed state consists of 48 atactic 20-monomeric-unit-long PNIPAM chains solvated with water whose amount corresponds to the activity of bulk water. For PNIPAM polymers we use the OPLS-based force field by Palivec *et al.*⁸⁷ For water we use the SPC/E water model,⁸⁸ and the OPLS-AA force field⁷² for penetrant molecules.

Diffusion. The diffusion in the collapsed state is studied by inserting 10–15 penetrant molecules of the same kind at random positions into equilibrated polymer structures (using 2–4 independent replicas) and tracking their mean square displacements (MSD). The diffusion coefficient is calculated from the linear fit of the MSD in the long-time limit. The necessary simulation times span up to 8000 ns for the slowest penetrants (NPe, CCl_4). The results are averaged over all the particles in the simulation box and over all replicas.

Simulation Details. The simulations are carried out using the GROMACS 5.1 simulation package⁸⁹ in the constant-pressure (NPT) ensemble, where the box sizes are independently adjusted in order to maintain the external pressure of 1 bar with a Berendsen barostat⁹⁰ with the time constant of 1 ps. The system temperature is controlled with a velocity-rescaling thermostat⁹¹ with a time constant of 0.1 ps. The Lennard-Jones (LJ) interactions are cut off at 1.0 nm.

Electrostatic interactions are treated using particle-mesh-Ewald methods with a 1.0 nm real-space cutoff.

Solvation Free Energies. The solvation free energies of the penetrant molecules are computed using the thermodynamic integration (TI) procedure,⁴⁰ where the penetrant's partial charges and LJ interactions between the penetrant molecule and other molecules are continuously switched off. For switching off the LJ interactions we use the “soft-core” LJ functions in order to avoid singularities when the potentials are about to vanish. All the TI calculations are performed using two to five independently equilibrated systems. Final results are averaged over all the particles in the simulation box and over all the systems. The transfer free energy of a penetrant from water into the PNIPAM phase is obtained as the difference of the solvation free energies between the two respective phases.

Accessible Surface Area. To evaluate the ASA of a given molecule, we consider the molecule as a union of fused van der Waals spheres increased by the standard probe radius of 0.14 nm. The ASA corresponds to the envelope area of the fused union of the spheres.⁹² Note that in the previous work⁴⁰ the molecular surface area was used instead, which is based on the same concept but with the probe radius of zero.

ASSOCIATED CONTENT

Supporting Information

The Supporting Information is available free of charge at <https://pubs.acs.org/doi/10.1021/acsnano.0c06319>.

Size scaling of diffusivity; glass transition temperature; chain relaxation time; comparison with the self-consistent cooperative hopping theory; compressibility of the collapsed PNIPAM state; size scaling of transfer free energy (PDF)

AUTHOR INFORMATION

Corresponding Authors

Matej Kanduč – Jožef Stefan Institute, SI-1000 Ljubljana, Slovenia; orcid.org/0000-0002-5307-7488; Email: matej.kanduc@ijs.si

Joachim Dzubiella – Applied Theoretical Physics–Computational Physics, Physikalisches Institut, Albert-Ludwigs-Universität Freiburg, D-79104 Freiburg, Germany; Research Group for Simulations of Energy Materials, Helmholtz-Zentrum Berlin für Materialien und Energie, D-14109 Berlin, Germany; orcid.org/0000-0001-6751-1487; Email: joachim.dzubiella@physik.uni-freiburg.de

Authors

Won Kyu Kim – Korea Institute for Advanced Study, Seoul 02455, Republic of Korea; orcid.org/0000-0002-6286-0925

Rafael Roa – Departamento de Física Aplicada I, Facultad de Ciencias, Universidad de Málaga, E-29071 Málaga, Spain; orcid.org/0000-0003-4439-418X

Complete contact information is available at: <https://pubs.acs.org/doi/10.1021/acsnano.0c06319>

Notes

The authors declare no competing financial interest.

ACKNOWLEDGMENTS

This project has received funding from the European Research Council (ERC) under the European Union's Horizon 2020 research and innovation program (Grant Agreement No.

646659-NANOREACTOR). J.D. acknowledges the support by the Deutsche Forschungsgemeinschaft (DFG, German Research Foundation) under Germany's Excellence Strategy—EXC-2193/1-390951807. M.K. acknowledges the financial support from the Slovenian Research Agency (research core funding No. P1-0055). W.K.K. acknowledges the support by a KIAS Individual Grant (CG076001) at Korea Institute for Advanced Study.

REFERENCES

- (1) Peer, D.; Karp, J. M.; Hong, S.; Farokhzad, O. C.; Margalit, R.; Langer, R. Nanocarriers as an Emerging Platform for Cancer Therapy. *Nat. Nanotechnol.* **2007**, *2*, 751.
- (2) Lu, Y.; Aimetti, A. A.; Langer, R.; Gu, Z. Bioresponsive Materials. *Nat. Rev. Mater.* **2017**, *2*, 1–17.
- (3) Li, J.; Mooney, D. J. Designing Hydrogels for Controlled Drug Delivery. *Nat. Rev. Mater.* **2016**, *1*, 16071.
- (4) Stuart, M. A. C.; Huck, W. T.; Genzer, J.; Muller, M.; Ober, C.; Stamm, M.; Sukhorukov, G. B.; Szleifer, I.; Tsukruk, V. V.; Urban, M.; Winnik, F. M.; Zauscher, S.; Luzinov, I.; Minko, S. Emerging Applications of Stimuli-Responsive Polymer Materials. *Nat. Mater.* **2010**, *9*, 101–113.
- (5) Koetting, M. C.; Peters, J. T.; Steichen, S. D.; Peppas, N. A. Stimulus-responsive Hydrogels: Theory, Modern Advances, and Applications. *Mater. Sci. Eng., R* **2015**, *93*, 1–49.
- (6) Feil, H.; Bae, Y. H.; Feijen, J.; Kim, S. W. Molecular Separation by Thermosensitive Hydrogel Membranes. *J. Membr. Sci.* **1991**, *64*, 283–294.
- (7) Aran, K.; Parades, J.; Rafi, M.; Yau, J. F.; Acharya, A. P.; Zibinsky, M.; Liepmann, D.; Murthy, N. Stimuli-Responsive Electrodes Detect Oxidative Stress and Liver Injury. *Adv. Mater.* **2015**, *27*, 1433–1436.
- (8) Li, D.; Zhang, X.; Yao, J.; Simon, G. P.; Wang, H. Stimuli-Responsive Polymer Hydrogels as a New Class of Draw Agent for Forward Osmosis Desalination. *Chem. Commun.* **2011**, *47*, 1710–1712.
- (9) Ali, W.; Gebert, B.; Hennecke, T.; Graf, K.; Ulbricht, M.; Gutmann, J. S. Design of Thermally Responsive Polymeric Hydrogels for Brackish Water Desalination: Effect of Architecture on Swelling, Deswelling, and Salt Rejection. *ACS Appl. Mater. Interfaces* **2015**, *7*, 15696–15706.
- (10) Buten, C.; Kortekaas, L.; Ravoo, B. J. Design of Active Interfaces Using Responsive Molecular Components. *Adv. Mater.* **2020**, *32*, 1904957.
- (11) Hoffman, A. S. Stimuli-Responsive Polymers: Biomedical Applications and Challenges for Clinical Translation. *Adv. Drug Delivery Rev.* **2013**, *65*, 10–16.
- (12) Ma, M.; Guo, L.; Anderson, D. G.; Langer, R. Bio-Inspired Polymer Composite Actuator and Generator Driven by Water Gradients. *Science* **2013**, *339*, 186–189.
- (13) Zhang, J.-T.; Wei, G.; Keller, T. F.; Gallagher, H.; Stötzl, C.; Müller, F. A.; Gottschaldt, M.; Schubert, U. S.; Jandt, K. D. Responsive Hybrid Polymeric/Metallic Nanoparticles for Catalytic Applications. *Macromol. Mater. Eng.* **2010**, *295*, 1049–1057.
- (14) Wu, S.; Dzubiella, J.; Kaiser, J.; Drechsler, M.; Guo, X.; Ballauff, M.; Lu, Y. Thermosensitive Au-PNIPAM Yolk-Shell Nanoparticles with Tunable Selectivity for Catalysis. *Angew. Chem., Int. Ed.* **2012**, *51*, 2229–2233.
- (15) Herves, P.; Perez-Lorenzo, M.; Liz-Marzan, L. M.; Dzubiella, J.; Lu, Y.; Ballauff, M. Catalysis by Metallic Nanoparticles in Aqueous Solution: Model Reactions. *Chem. Soc. Rev.* **2012**, *41*, 5577–5587.
- (16) Roa, R.; Angioletti-Uberti, S.; Lu, Y.; Dzubiella, J.; Piazza, F.; Ballauff, M. Catalysis by Metallic Nanoparticles in Solution: Thermosensitive Microgels as Nanoreactors. *Z. Phys. Chem.* **2018**, *232*, 773–803.
- (17) Dong, L.-C.; Hoffman, A. S. Synthesis and Application of Thermally Reversible Heterogels for Drug Delivery. *J. Controlled Release* **1990**, *13*, 21–31.
- (18) Peppas, N. A. Hydrogels and Drug Delivery. *Curr. Opin. Colloid Interface Sci.* **1997**, *2*, 531–537.
- (19) Lu, Y.; Mei, Y.; Drechsler, M.; Ballauff, M. Thermosensitive Core-Shell Particles as Carriers for Ag Nanoparticles: Modulating the Catalytic Activity by a Phase Transition in Networks. *Angew. Chem., Int. Ed.* **2006**, *45*, 813–816.
- (20) Carregal-Romero, S.; Buurma, N. J.; Pérez-Juste, J.; Liz-Marzán, L. M.; Hervés, P. Catalysis by Au@pNIPAM Nanocomposites: Effect of the Cross-Linking Density. *Chem. Mater.* **2010**, *22*, 3051–3059.
- (21) Angioletti-Uberti, S.; Lu, Y.; Ballauff, M.; Dzubiella, J. Theory of Solvation-Controlled Reactions in Stimuli-Responsive Nano-reactors. *J. Phys. Chem. C* **2015**, *119*, 15723–15730.
- (22) Roa, R.; Kim, W. K.; Kanduč, M.; Dzubiella, J.; Angioletti-Uberti, S. Catalyzed Bimolecular Reactions in Responsive Nano-reactors. *ACS Catal.* **2017**, *7*, 5604–5611.
- (23) Paul, D. R. The Solution-Diffusion Model for Swollen Membranes. *Sep. Purif. Methods* **1976**, *5*, 33–50.
- (24) Lonsdale, H.; Merten, U.; Riley, R. Transport Properties of Cellulose Acetate Osmotic Membranes. *J. Appl. Polym. Sci.* **1965**, *9*, 1341–1362.
- (25) Wijmans, J. G.; Baker, R. W. The Solution-Diffusion Model: a Review. *J. Membr. Sci.* **1995**, *107*, 1–21.
- (26) Kucukpinar, E.; Doruker, P. Molecular Simulations of Small Gas Diffusion and Solubility in Copolymers of Styrene. *Polymer* **2003**, *44*, 3607–3620.
- (27) Ban, S.; Huang, C.; Yuan, X.-Z.; Wang, H. Molecular Simulation of gas Adsorption, Diffusion, and Permeation in Hydrated Nafion Membranes. *J. Phys. Chem. B* **2011**, *115*, 11352–11358.
- (28) Kim, W. K.; Kanduč, M.; Roa, R.; Dzubiella, J. Tuning the Permeability of Dense Membranes by Shaping Nanoscale Potentials. *Phys. Rev. Lett.* **2019**, *122*, 108001.
- (29) Palasis, M.; Gehrke, S. H. Permeability of Responsive Poly(N-isopropylacrylamide) Gel to Solutes. *J. Controlled Release* **1992**, *18*, 1–11.
- (30) Kim, W. K.; Chudoba, R.; Milster, S.; Roa, R.; Kanduč, M.; Dzubiella, J. Tuning the Selective Permeability of Polydisperse Polymer Networks. *Soft Matter* **2020**, *16*, 8144–8154.
- (31) Lee, W. Selection of Barrier Materials from Molecular Structure. *Polym. Eng. Sci.* **1980**, *20*, 65–69.
- (32) Salame, M. Prediction of Gas Barrier Properties of High Polymers. *Polym. Eng. Sci.* **1986**, *26*, 1543–1546.
- (33) Amsden, B. Solute Diffusion within Hydrogels. Mechanisms and Models. *Macromolecules* **1998**, *31*, 8382–8395.
- (34) Masaro, L.; Zhu, X. Physical Models of Diffusion for Polymer Solutions, Gels and Solids. *Prog. Polym. Sci.* **1999**, *24*, 731–775.
- (35) Müller-Plathe, F. Permeation of Polymers—a Computational Approach. *Acta Polym.* **1994**, *45*, 259–293.
- (36) Richbourg, N. R.; Peppas, N. A. The Swollen Polymer Network Hypothesis: Quantitative Models of Hydrogel Swelling, Stiffness, and Solute Transport. *Prog. Polym. Sci.* **2020**, *105*, 101243.
- (37) Halperin, A.; Kröger, M.; Winnik, F. M. Poly (N-Isopropylacrylamide) Phase Diagrams: Fifty Years of Research. *Angew. Chem., Int. Ed.* **2015**, *54*, 15342–15367.
- (38) Kanduč, M.; Chudoba, R.; Palczynski, K.; Kim, W. K.; Roa, R.; Dzubiella, J. Selective Solute Adsorption and Partitioning around Single PNIPAM Chains. *Phys. Chem. Chem. Phys.* **2017**, *19*, 5906–5916.
- (39) Kanduč, M.; Kim, W. K.; Roa, R.; Dzubiella, J. Selective Molecular Transport in Thermo-Responsive Polymer Membranes: Role of Nanoscale Hydration and Fluctuations. *Macromolecules* **2018**, *51*, 4853–4864.
- (40) Kanduč, M.; Kim, W. K.; Roa, R.; Dzubiella, J. Transfer Free Energies and Partitioning of Small Molecules in Collapsed PNIPAM Polymers. *J. Phys. Chem. B* **2019**, *123*, 720–728.
- (41) Kanduč, M.; Kim, W. K.; Roa, R.; Dzubiella, J. Modeling of Stimuli-Responsive Nanoreactors: Rational Rate Control Towards the Design of Colloidal Enzymes. *Mol. Syst. Des. Eng.* **2020**, *5*, 602–619.
- (42) Wunder, S.; Polzer, F.; Lu, Y.; Mei, Y.; Ballauff, M. Kinetic Analysis of Catalytic Reduction of 4-Nitrophenol by Metallic

Nanoparticles Immobilized in Spherical Polyelectrolyte Brushes. *J. Phys. Chem. C* **2010**, *114*, 8814–8820.

(43) Zhao, P.; Feng, X.; Huang, D.; Yang, G.; Astruc, D. Basic Concepts and Recent Advances in Nitrophenol Reduction by Gold- and Other Transition Metal Nanoparticles. *Coord. Chem. Rev.* **2015**, *287*, 114–136.

(44) Milster, S.; Chudoba, R.; Kanduč, M.; Dzubiella, J. Cross-Linker Effect on Solute Adsorption in Swollen Thermoresponsive Polymer Networks. *Phys. Chem. Chem. Phys.* **2019**, *21*, 6588.

(45) Edward, J. T. Molecular Volumes and the Stokes-Einstein Equation. *J. Chem. Educ.* **1970**, *47*, 261.

(46) Lielig, O.; Ribbeck, K. Biological hydrogels as selective diffusion barriers. *Trends Cell Biol.* **2011**, *21*, 543–551.

(47) Hansing, J.; Duke, J. R., III; Fryman, E. B.; DeRouchey, J. E.; Netz, R. R. Particle Diffusion in Polymeric Hydrogels with Mixed Attractive and Repulsive Interactions. *Nano Lett.* **2018**, *18*, 5248–5256.

(48) Mackie, J.; Meares, P. The Diffusion of Electrolytes in a Cation-Exchange Resin Membrane I. Theoretical. *Proc. R. Soc. London, Ser. A* **1955**, *232*, 498–509.

(49) Berg, O. G. Effective Diffusion Rate through a Polymer Network: Influence of Nonspecific Binding and Intersegment Transfer. *Biopolymers* **1986**, *25*, 811–821.

(50) Sasaki, S.; Koga, S.; Maeda, H. Dielectric Properties of Collapsing Hydrogels. *Macromolecules* **1999**, *32*, 4619–4624.

(51) Raccis, R.; Roskamp, R.; Hopp, I.; Menges, B.; Koynov, K.; Jonas, U.; Knoll, W.; Butt, H.-J.; Fytas, G. Probing Mobility and Structural Inhomogeneities in Grafted Hydrogel Films by Fluorescence Correlation Spectroscopy. *Soft Matter* **2011**, *7*, 7042–7053.

(52) Kaneko, Y.; Yoshida, R.; Sakai, K.; Sakurai, Y.; Okano, T. Temperature-Responsive Shrinking Kinetics of Poly (N-isopropylacrylamide) Copolymer Gels with Hydrophilic and Hydrophobic Comonomers. *J. Membr. Sci.* **1995**, *101*, 13–22.

(53) Dong, L. C.; Hoffman, A. S. Thermally Reversible Hydrogels: III. Immobilization of Enzymes for Feedback Reaction Control. *J. Controlled Release* **1986**, *4*, 223–227.

(54) Tamai, Y.; Tanaka, H.; Nakanishi, K. Molecular Simulation of Permeation of Small Penetrants through Membranes. I. Diffusion Coefficients. *Macromolecules* **1994**, *27*, 4498–4508.

(55) Fukuda, M. Clustering of Water in Polyethylene: A Molecular-Dynamics Simulation. *J. Chem. Phys.* **1998**, *109*, 6476–6485.

(56) Sok, R.; Berendsen, H.; van Gunsteren, W. Molecular Dynamics Simulation of the Transport of Small Molecules Across a Polymer Membrane. *J. Chem. Phys.* **1992**, *96*, 4699–4704.

(57) Takeuchi, H. A Jump Motion of Small Molecules in Glassy Polymers: A Molecular Dynamics Simulation. *J. Chem. Phys.* **1990**, *93*, 2062–2067.

(58) Müller-Plathe, F. Diffusion of Penetrants in Amorphous Polymers: A molecular Dynamics Study. *J. Chem. Phys.* **1991**, *94*, 3192–3199.

(59) Ghugare, S. V.; Chiessi, E.; Telling, M. T.; Deriu, A.; Gerelli, Y.; Wuttke, J.; Paradossi, G. Structure and Dynamics of a Thermoresponsive Microgel Around Its Volume Phase Transition Temperature. *J. Phys. Chem. B* **2010**, *114*, 10285–10293.

(60) Philipp, M.; Kyriakos, K.; Silvi, L.; Lohstroh, W.; Petry, W.; Krüger, J. K.; Papadakis, C. M.; Müller-Buschbaum, P. From Molecular Dehydration To Excess Volumes of Phase-Separating PNIPAM Solutions. *J. Phys. Chem. B* **2014**, *118*, 4253–4260.

(61) Falk, K.; Savio, D.; Moseler, M. Nonempirical Free Volume Viscosity Model for Alkane Lubricants Under Severe Pressures. *Phys. Rev. Lett.* **2020**, *124*, 105501.

(62) Michaels, A. S.; Bixler, H. J. Flow of Gases Through Polyethylene. *J. Polym. Sci.* **1961**, *50*, 413–439.

(63) Cai, L.-H.; Panyukov, S.; Rubinstein, M. Hopping Diffusion of Nanoparticles in Polymer Matrices. *Macromolecules* **2015**, *48*, 847–862.

(64) Zhang, R.; Schweizer, K. S. Correlated Matrix-Fluctuation-Mediated Activated Transport of Dilute Penetrants in Glass-Forming Liquids and Suspensions. *J. Chem. Phys.* **2017**, *146*, 194906.

(65) Lustig, S. R.; Peppas, N. A. Solute Diffusion in Swollen Membranes. IX. Scaling Laws for Solute Diffusion in Gels. *J. Appl. Polym. Sci.* **1988**, *36*, 735–747.

(66) Peppas, N. A.; Reinhart, C. T. Solute Diffusion in Swollen Membranes. Part I. A New Theory. *J. Membr. Sci.* **1983**, *15*, 275–287.

(67) Freeman, B. D. Basis of Permeability/Selectivity Tradeoff Relations in Polymeric Gas Separation Membranes. *Macromolecules* **1999**, *32*, 375–380.

(68) Zhang, K.; Kumar, S. K. Molecular Simulations of Solute Transport in Polymer Melts. *ACS Macro Lett.* **2017**, *6*, 864–868.

(69) Meng, D.; Zhang, K.; Kumar, S. K. Size-Dependent Penetrant Diffusion in Polymer Glasses. *Soft Matter* **2018**, *14*, 4226–4230.

(70) Zhang, K.; Meng, D.; Müller-Plathe, F.; Kumar, S. K. Coarse-Grained Molecular Dynamics Simulation of Activated Penetrant Transport in Glassy Polymers. *Soft Matter* **2018**, *14*, 440–447.

(71) Lide, D. R. *CRC Handbook of Chemistry and Physics*; CRC Press, 2004; Vol. 85.

(72) Jorgensen, W. L.; Tirado-Rives, J. The OPLS [Optimized Potentials for Liquid Simulations] Potential Functions for Proteins, Energy Minimization for Crystals of Cyclic Peptides and Crambin. *J. Am. Chem. Soc.* **1988**, *110*, 1657–1666.

(73) Tanford, C. Interfacial Free Energy and the Hydrophobic Effect. *Proc. Natl. Acad. Sci. U. S. A.* **1979**, *76*, 4175–4176.

(74) Ashbaugh, H. S.; Pratt, L. R. Colloquium: Scaled Particle Theory and the Length Scales of Hydrophobicity. *Rev. Mod. Phys.* **2006**, *78*, 159.

(75) Guilherme, M.; Silva, R.; Girotto, E.; Rubira, A.; Muniz, E. Hydrogels Based on PAAm Network with PNIPAAm Included: Hydrophilic–Hydrophobic Transition Measured by the Partition of Orange II and Methylene Blue in Water. *Polymer* **2003**, *44*, 4213–4219.

(76) Sedlmeier, F.; Netz, R. R. The Spontaneous Curvature of the Water–Hydrophobe Interface. *J. Chem. Phys.* **2012**, *137*, 135102.

(77) Ghosal, K.; Freeman, B. D. Gas Separation Using Polymer Membranes: an Overview. *Polym. Adv. Technol.* **1994**, *5*, 673–697.

(78) Harris, R. C.; Pettitt, B. M. Effects of Geometry and Chemistry on Hydrophobic Solvation. *Proc. Natl. Acad. Sci. U. S. A.* **2014**, *111*, 14681–14686.

(79) Chandler, D. Interfaces and the driving force of hydrophobic assembly. *Nature* **2005**, *437*, 640–647.

(80) Al-Awqati, Q. One Hundred Years of Membrane Permeability: Does Overton Still Rule? *Nat. Cell Biol.* **1999**, *1*, E201–E202.

(81) Nagle, J. F.; Mathai, J. C.; Zeidel, M. L.; Tristram-Nagle, S. Theory of Passive Permeability Through Lipid Bilayers. *J. Gen. Physiol.* **2008**, *131*, 77–85.

(82) Bell, D.; Roedder, D.; Wessling, M. Monodisperse Porous Microspheres with pH-Responsive Permeability and Reactivity. *ACS Appl. Polym. Mater.* **2020**, *2*, 932.

(83) Geise, G. M.; Paul, D. R.; Freeman, B. D. Fundamental Water and Salt Transport Properties of Polymeric Materials. *Prog. Polym. Sci.* **2014**, *39*, 1–42.

(84) Pandey, P.; Chauhan, R. Membranes for Gas Separation. *Prog. Polym. Sci.* **2001**, *26*, 853–893.

(85) Park, H. B.; Kamcev, J.; Robeson, L. M.; Elimelech, M.; Freeman, B. D. Maximizing the Right Stuff: The Trade-off Between Membrane Permeability and Selectivity. *Science* **2017**, *356*, eaab0530.

(86) Kanduč, M.; Kim, W. K.; Roa, R.; Dzubiella, J. Aqueous Nanoclusters Govern Ion Partitioning in Dense Polymer Membranes. *ACS Nano* **2019**, *13*, 11224–11234.

(87) Palivec, V.; Zadrzil, D.; Heyda, J. All-Atom REMD Simulation of Poly-N-Isopropylacrylamide Thermodynamics in Water: a Model with a Distinct 2-State Behavior. *arXiv preprint arXiv:1806.05592* **2018**.

(88) Berendsen, H. J. C.; Grigera, J. R.; Straatsma, T. P. The Missing Term in Effective Pair Potentials. *J. Phys. Chem.* **1987**, *91*, 6269–6271.

(89) van der Spoel, D.; Lindahl, E.; Hess, B.; Groenhof, G.; Mark, A. E.; Berendsen, H. J. C. GROMACS: Fast, Flexible, and Free. *J. Comput. Chem.* **2005**, *26*, 1701–1718.

(90) Berendsen, H. J. C.; Postma, J. P. M.; van Gunsteren, W. F.; DiNola, A.; Haak, J. R. Molecular Dynamics with Coupling to an External Bath. *J. Chem. Phys.* **1984**, *81*, 3684–3690.

(91) Bussi, G.; Donadio, D.; Parrinello, M. Canonical Sampling through Velocity Rescaling. *J. Chem. Phys.* **2007**, *126*, 014101.

(92) Shrake, A.; Rupley, J. Environment and Exposure to Solvent of Protein Atoms. Lysozyme and Insulin. *J. Mol. Biol.* **1973**, *79*, 351–371.